Long-range interactions between rubidium and potassium Rydberg atoms

Nolan Samboy*

Department of Physical and Biological Sciences, Western New England University, 1215 Wilbraham Road, Springfield, Massachusetts 01119, USA

(Received 24 February 2016; revised manuscript received 15 January 2017; published 15 March 2017)

We investigate the long-range, two-body interactions between rubidium and potassium atoms in highly excited ($n = 70$) Rydberg states. After establishing properly symmetrized asymptotic basis states, we diagonalize an interaction Hamiltonian consisting of the standard Coulombic potential expansion and atomic fine structure to calculate electronic potential energy curves. We find that when both atoms are excited to either the $70s$ state or the $70p$ state, both the $\Omega = 0^+$ symmetry interactions and the $\Omega = 0^-$ symmetry interactions demonstrate a deep potential well capable of supporting many bound levels; the sizes of the corresponding dimer states are of the order of 2.25 μm. We establish n-scaling relations for the equilibrium separation R_e and the dissociation energy D_e and find these relations to be consistent with similar calculations involving the homonuclear interactions between rubidium and cesium. We discuss the specific effects of ℓ mixing and the exact composition of the calculated potential well via the expansion coefficients of the asymptotic basis states. Finally, we apply a Landau-Zener treatment to show that the dimer states are stable with respect to predissociation.

DOI: 10.1103/PhysRevA.95.032702

I. INTRODUCTION

With the advent of laser cooling and atomic trapping, the investigation of Rydberg atoms experienced a renaissance in the late 20th century, which has led to many experimental discoveries and theoretical predictions. Exaggerated properties (long lifetimes, large cross sections, very large polarizabilities, etc.) [1] make the Rydberg atom especially responsive to external electric and magnetic fields, as well as to other Rydberg atoms.

Under ultracold conditions, the dipole-dipole interactions between two Rydberg atoms is not masked by thermal motion, and so interactions can occur at very long range [2,3]. These interactions have manifested in a variety of results including molecular resonance excitation spectra [4,5], "exotic" molecules (*trilobite* states [6,7] and *macrodimer* states [8–11]), and the excitation-blockade effect [12]. All of these works uniquely illustrate the potential for applications in quantum information processes (see [13], and more recently [14], for excellent comprehensive reviews of Rydberg physics research).

Within the last few years, the focus of study involving Rydberg systems has moved toward few-body interactions. For example, there have been proposals for long-range interactions between one Rydberg atom and multiple ground-state atoms [15–18], as well as for bound states between three Rydberg atoms [19–21]. Currently, Rydberg states involving alkaline-earth elements are also being investigated [22–24], with the goal of forming Rydberg-Rydberg pairs at large interatomic separations. The inner valence electrons in each atom of such a dimer would offer an approach to probe and manipulate Rydberg systems.

The works mentioned here have all been with regard to homonuclear interactions; to the author's knowledge, Rydberg interactions between multiple species have not yet been considered. Fairly recently, photoassociation between different alkali species in the ground state (^{39}K ^{85}Rb) was achieved [25,26]. In principle, such techniques could be applied to Rydberg states of these atoms to probe resonance features; this paper aims to assist in this effort.

We discuss an approach for calculating long-range Rydberg interactions between two different alkali atoms; although we specifically discuss calculations involving rubidium and potassium, the theory can be applied to any heteronuclear alkali pairing. Such results are relevant to the continuing work in ultracold physics and chemistry, specifically with regard to the "exotic" Rydberg dimer states. Please note: Except where otherwise indicated, atomic units are used throughout.

II. LONG-RANGE INTERACTIONS

Neutral, alkali Rydberg atoms are convenient to explore because they are well treated using the semiclassical Bohr model (with the quantum defect correction) [1]. In addition, the neutrality of the atoms ensures minimal interactions with the environment while in the ground state [27,28], and the translational motion of the nuclei can be neglected at ultracold temperatures [2,3].

When the distance between the two interacting Rydberg atoms is greater than the Le-Roy radius [29],

$$R_{\mathrm{LR}} = 2\left[\langle n_1\ell_1|r^2|n_1\ell_1\rangle^{1/2} + \langle n_2\ell_2|r^2|n_2\ell_2\rangle^{1/2}\right], \quad (1)$$

the interactions are considered "long range" and there is no overlap of the two electron clouds. The potential energy of the interaction is then described by that of two, well-separated charge distributions. For the case of Rydberg atoms, each charge distribution is effectively a two particle system: a $+1$ nuclear core and a single, highly excited valence electron.

Figure 1 schematically represents two such interacting Rydberg atoms: electron 1 is a distance r_1 from core A, and electron 2 is a distance r_2 from core B. In the long-range scenario, the nuclear distance R is much larger than both r_1 and r_2. When the two nuclear cores are assumed to be fixed in space (no kinetic energy), then the interaction Hamiltonian is

*nolan.samboy@wne.edu

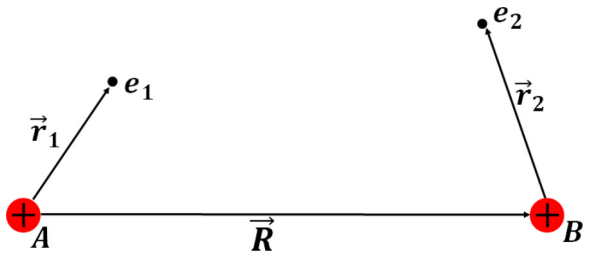

FIG. 1. Two Rydberg atoms well separated from each other; each consists of a +1 nuclear core and a single, highly excited valence electron e_i. Here, the nuclear distance R is greater than the LeRoy radius (see text) and thus much larger than either electron's distance r_i from its respective nuclear core.

expressed in atomic units as

$$\hat{H} = \hat{H}_A + \hat{H}_B + \hat{V}_{\text{int}} \ , \tag{2}$$

where $\hat{H}_i$ contains the kinetic and potential energies of atom i and $\hat{V}_{\text{int}}$ is the Coulombic potential energy combinations of the two nuclei and the two electrons, given in atomic units as

$$\hat{V}_{\text{int}} = \frac{1}{R} - \frac{1}{|\vec{R}+\vec{r}_2|} - \frac{1}{|\vec{R}-\vec{r}_1|} + \frac{1}{|\vec{R}+\vec{r}_2-\vec{r}_1|} \ . \tag{3}$$

A. Basis states

Given a nonrelativistic Schrödinger equation, the fine-structure energy splitting is a result of the spin-orbit coupling between the total spin angular momentum of the dimer $\vec{S}$ and the total orbital angular momentum of the dimer $\vec{L}$. When nuclear rotation is neglected, Hund's case (c) is the appropriate molecular basis where the good quantum numbers are the total angular momentum of the dimer $\vec{J} = \vec{L} + \vec{S}$ and its projection Ω along the internuclear axis.

We adopt a typical approach and assume the dimer wave function to be a product of two atomic wave functions. Under the Born-Oppenheimer approximation, each atomic wave function is solely described by the quantum state of its valence electron 1 (2) about the respective nucleus A (B). In the coupled basis representation, each atom possesses total atomic angular momentum $\vec{j}_i = \vec{\ell}_i + \vec{s}_i$, where $\vec{\ell}_i$ is the orbital angular momentum of atom i and $\vec{s}_i$ is the spin angular momentum of atom i. The dimer wave functions are thus expressed as $|1A\rangle \equiv |n_1,\ell_1,j_1,m_{j_1}\rangle_A$ and $|2B\rangle \equiv |n_2,\ell_2,j_2,\Omega - m_{j_1}\rangle_B$. Here n_i is the principal quantum number of atom i, ℓ_i is the orbital angular momentum quantum number of atom i, and m_{j_i} is the projection of the total atomic angular momentum $\vec{j}_i$ of atom i onto the internuclear axis (chosen in the z direction for convenience).

For the interactions considered here, the fine-structure energies are too high for perturbation theory to be applicable. Thus, we directly diagonalize the interaction Hamiltonian at successive values of R to compute electronic potential energy curves, as done in [30] and [31]. This approach has proven to be more successful at explaining experimental resonance features [4] because it more accurately describes the intricate mixing of the electrons' angular momentum characters (ℓ mixing).

To facilitate faster computational times, we exploit molecular symmetries to construct symmetrized molecular wave functions, as done in [9], [10], [30], and [31]. Although the heteronuclear dimer does not possess the inversion symmetry of its homonuclear counterpart, the total wave function does remain antisymmetric with respect to electron exchange. Therefore, as long as Eq. (1) is satisfied, the properly symmetrized molecular wave function is given by

$$|1A,2B;\Omega\rangle \sim \frac{1}{\sqrt{2}}(|1A\rangle|2B\rangle - |2B\rangle|1A\rangle). \tag{4}$$

For $\Omega = 0$, reflection of the dimer through a plane containing the internuclear axis leads to wave functions that are either symmetric or antisymmetric with respect to the reflection operator $\hat{\sigma}_v$. Furthermore, these wave functions have nondegenerate energy values and must be uniquely defined. We distinguish between the two based on how $\hat{\sigma}_v$ operates on (4),

$$|1A,2B;\Omega = 0^{\pm}\rangle = \left(\frac{1 \pm \hat{\sigma}_v}{\sqrt{2}}\right)|1A,2B;\Omega = 0\rangle \ , \tag{5}$$

where $\hat{\sigma}_v$ behaves according to the following rules [32,33]:

$$\hat{\sigma}_v|\Lambda\rangle = (-1)^{\Lambda}|-\Lambda\rangle, \tag{6}$$

$$\hat{\sigma}_v|S,M_S\rangle = (-1)^{S-M_S}|S,-M_S\rangle \ . \tag{7}$$

B. Basis sets

In general, any basis set (defined by Ω) will consist of molecular states corresponding to those asymptotes with significant coupling both to the Rydberg-Rydberg asymptotic level being considered and to other nearby states. We gauge the relative interaction strengths of local asymptotes based on their contributions to the the $C_6 \sim \frac{\langle\phi_1|r|\phi_2\rangle\langle\phi_3|r|\phi_4\rangle)^2}{(E_1+E_3)-(E_2+E_4)}$ (dipole-dipole) and $C_5 \sim \langle\phi_1|r^2|\phi_2\rangle\langle\phi_3|r^2|\phi_4\rangle$ (quadrupole-quadrupole) coefficients of the molecular Rydberg state being considered. In these expressions, each E_i is the asymptotic energy of atom i in state ϕ_i and $\langle\phi_i|r^k|\phi_j\rangle$ is the radial matrix element between atom i and atom j.

As mentioned before, the C_i coefficients (perturbation theory) are not sufficient to properly describe the long-range Rydberg-Rydberg interaction picture detailed in this work; however, such analysis does accurately assess which asymptotes provide strong coupling and which do not. For example, if we consider the $70^{(\text{K})}s + 70^{(\text{Rb})}s$ Rydberg level, the largest contribution to the C_6 coefficient comes from the $69^{(\text{K})}p + 70^{(\text{Rb})}p$ state (8.89317×10^{14}), while the largest contribution to the C_5 coefficient comes from the $67^{(\text{K})}d + 69^{(\text{Rb})}d$ state (3.8039×10^{15}) and the $68^{(\text{K})}d + 70^{(\text{Rb})}d$ state (2.4682×10^{15}). To provide some contrast, the contribution of the $71^{(\text{K})}p + 71^{(\text{Rb})}p$ state to the C_6 coefficient is 2.51707×10^9, while the contribution of the $72^{(\text{K})}d + 72^{(\text{Rb})}d$ state to the C_5 coefficient is 3.80343×10^{11}. Since the contributions of these states are 4 or 5 orders of magnitude smaller, they are not included in the basis.

To construct a more complete basis set, we examine asymptotes in the vicinity ($\sim\pm$20 GHz) of the molecular Rydberg level being considered and we find in Table I that the dipole strength between two atomic Rydberg states decays

TABLE I. Dipole matrix elements for atomic transitions from Rb $70s$ and (right) K $70s$. Values for the two largest elements for each atomic species are in boldface and note the rapid decrease in coupling strength as $\Delta n = |n_1 - n_2|$ increases.

Rubidium	Potassium
$\langle 70s\|r\|74p_{3/2}\rangle = 94.064$	$\langle 70s\|r\|74p_{3/2}\rangle = 87.093$
$\langle 70s\|r\|73p_{3/2}\rangle = -144.19$	$\langle 70s\|r\|73p_{3/2}\rangle = -134.41$
$\langle 70s\|r\|72p_{3/2}\rangle = 258.08$	$\langle 70s\|r\|72p_{3/2}\rangle = 243.23$
$\langle 70s\|r\|71p_{3/2}\rangle = -639.57$	$\langle 70s\|r\|71p_{3/2}\rangle = -616.30$
$\langle 70s\|r\|70p_{3/2}\rangle =$ **5081.6**	$\langle 70s\|r\|70p_{3/2}\rangle =$ **5353.1**
$\langle 70s\|r\|69p_{3/2}\rangle =$ **4807.8**	$\langle 70s\|r\|69p_{3/2}\rangle =$ **4810.7**
$\langle 70s\|r\|68p_{3/2}\rangle = -649.29$	$\langle 70s\|r\|68p_{3/2}\rangle = -696.92$
$\langle 70s\|r\|67p_{3/2}\rangle = 262.07$	$\langle 70s\|r\|67p_{3/2}\rangle = 285.92$
$\langle 70s\|r\|66p_{3/2}\rangle = -144.50$	$\langle 70s\|r\|66p_{3/2}\rangle = -158.83$

rapidly with the relative difference in their principal quantum numbers: $\Delta n \equiv |n_1 - n_2|$. Note: This table details specific results for transitions from rubidium in the $70s$ state and from potassium in the $70s$ state, but similar behaviors are found for transitions from any excited $n\ell$ Rydberg state. Due to the sharp decline in the coupling strengths, we only consider nearby asymptotic levels whose two constituent atoms have n_i values in the range $(n-3) \leqslant n_i \leqslant (n+3)$, where n is the principal quantum number of the excited Rydberg state for each atom ($n = 70$ for all tabulated results in this paper).

Table II lists the relevant molecular levels near the $70s + 70s$ asymptote and the $70p + 70p$ asymptote; the properly symmetrized states corresponding to these molecular levels comprise the appropriate basis sets.

C. Interaction Hamiltonian

Under the Born-Oppenheimer approximation, diagonalization of the interaction Hamiltonian [Eq. (2)] results in a set of electronic energies with regard to a fixed nuclear separation R. A complete set of electronic energy curves can be calculated by diagonalizing a unique Hamiltonian matrix at varying values of R.

TABLE II. Molecular asymptotes included in the basis sets for long-range interactions between rubidium and potassium. In the first column, each atom was excited to the $70s$ Rydberg state; in the second column, to the $70p$ Rydberg state.

K($70s$)-Rb($70s$)	K($70p$)-Rb($70p$)
$68^{(K)}d + 70^{(Rb)}s$	$67^{(K)}f + 71^{(Rb)}p$
$69^{(K)}s + 69^{(Rb)}d$	$68^{(K)}f + 70^{(Rb)}p$
$68^{(K)}p + 71^{(Rb)}p$	$68^{(K)}d + 69^{(Rb)}d$
$69^{(K)}p + 70^{(Rb)}p$	$69^{(K)}s + 70^{(Rb)}d$
$69^{(K)}s + 71^{(Rb)}s$	$67^{(K)}d + 72^{(Rb)}s$
$70^{(K)}s + 70^{(Rb)}s$	$69^{(K)}d + 70^{(Rb)}s$
$68^{(K)}d + 69^{(Rb)}d$	$68^{(K)}d + 71^{(Rb)}s$
	$69^{(K)}p + 71^{(Rb)}p$
	$70^{(K)}p + 70^{(Rb)}p$
	$69^{(K)}s + 72^{(Rb)}s$
	$70^{(K)}s + 71^{(Rb)}s$
	$67^{(K)}f + 69^{(Rb)}f$
	$68^{(K)}f + 68^{(Rb)}f$

A convenient approach for long-range Rydberg investigations is to express the Coulombic potential energy expression [Eq. (3)] as a multipole expansion in inverse powers of R [34–36]; the expansion is further simplified if we assume that $\vec{\boldsymbol{R}}$ lies along a z axis, common to both Rydberg atoms [37]:

$$\hat{V}_{\rm int} \equiv V_L(R) = \sum_{L=0}^{\infty}(-1)^L \frac{4\pi}{R^{2L+1}(2L+1)} r_1^L r_2^L \times \sum_{m=-L}^{L} B_{2L}^{L+m}\, Y_L^m(\hat{\boldsymbol{r}}_1)\, Y_L^{-m}(\hat{\boldsymbol{r}}_2)\,. \quad (8)$$

Here, $B_n^k \equiv \frac{n!}{k!(n-k)!}$ is the binomial coefficient, $Y_L^m(\hat{\boldsymbol{r}}_i)$ is a spherical harmonic describing the angular position of electron i with position $\vec{\boldsymbol{r}}_i$ from its nuclear center, L labels the (2^L) multipole moment ($L = 1$ for dipolar, $L = 2$ for quadrupolar, etc.), and R is the internuclear distance. The advantage of such an expansion is that the expression can be truncated such that only meaningful terms are kept; this significantly reduces the computation time.

When the Hamiltonian is diagonalized, the expectation value of each term in the energy expansion is proportional to $\frac{\langle r_1^L\rangle\langle r_2^L\rangle}{R^{2L+1}}$; for Rydberg atoms, each radial element scales as $\langle r^L\rangle \sim n^{2L}$ [1]. Thus, dipole-dipole interactions scale as $\sim\frac{n^4}{R^3}$, quadrupole-quadrupole interactions scale as $\sim\frac{n^8}{R^5}$ and so on. For the internuclear spacings considered here, $R \approx n^{5/2}$, so the dipole-dipole coupling strength is $\sim n^{-7/2}$ and the quadrupole-quadrupole coupling strength is $\sim n^{-9/2}$.

Typically, dipole-dipole interactions dominate the long-range Rydberg-Rydberg interactions, but it has been shown [31,38] that quadrupole-quadrupole couplings can also be significant to the interaction picture. To date, octupole-octupole interactions have not been shown to be relevant in long-range Rydberg interactions, so we do not consider them here. Based on the scaling relations shown above, such a term would be a factor of n^{-1} less than the quadrupole-quadrupole term and a factor of n^{-2} less than the dipole-dipole term.

Because the molecular basis states are linear combinations of atomic states determined through symmetry considerations [see Eq. (4)], each matrix element in the interaction Hamiltonian is actually a combination of multiple interaction terms:

$$\begin{aligned}\langle 1A,2B;\Omega|\hat{H}|3A,4B;\Omega\rangle \sim\ & \langle 1A,2B|\hat{H}|3A,4B\rangle \\ & - \langle 1A,2B|\hat{H}|4A,3B\rangle \\ & - \langle 2A,1B|\hat{H}|3A;4B\rangle \\ & + \langle 2A,1B|\hat{H}|4A;3B\rangle\,. \quad (9)\end{aligned}$$

For the $\Omega = 0$ case, Eq. (5) is also applied, resulting in additional terms. Since the normalization factor varies with state definitions and symmetry considerations, it is not stated explicitly in (9). Normalization factors are included in calculations, however. In this notation, $|1A,2B\rangle = |n_1,\ell_1,j_1,m_{j_1}\rangle_A|n_2,\ell_2,j_2,\Omega - m_{j_1}\rangle_B$, and so on.

An analytical expression for any given term in the matrix element is found to be

$$\begin{aligned}
&\langle 1A,2B|V_L(R)|3A,4B\rangle \\
&= (-1)^{L-1-\Omega+j_{\rm tot}}\sqrt{\hat{\ell}_1\hat{\ell}_2\hat{\ell}_3\hat{\ell}_4\hat{j}_1\hat{j}_2\hat{j}_3\hat{j}_4}\;\frac{\mathcal{R}^L_{13,A}\,\mathcal{R}^L_{24,B}}{R^{2L+1}} \\
&\times\begin{pmatrix}\ell_1 & L & \ell_3\\ 0 & 0 & 0\end{pmatrix}\begin{pmatrix}\ell_2 & L & \ell_4\\ 0 & 0 & 0\end{pmatrix} \\
&\times\begin{Bmatrix}j_1 & L & j_3\\ \ell_3 & \frac{1}{2} & \ell_1\end{Bmatrix}\begin{Bmatrix}j_2 & L & j_4\\ \ell_4 & \frac{1}{2} & \ell_2\end{Bmatrix} \\
&\times\sum_{m=-L}^{L} B_{2L}^{L+m}\begin{pmatrix}j_1 & L & j_3\\ -m_{j_1} & m & m_{j_3}\end{pmatrix} \\
&\times\begin{pmatrix}j_2 & L & j_4\\ -m_{j_2} & -m & m_{j_4}\end{pmatrix}, \qquad (10)
\end{aligned}$$

where $j_{\rm tot} = j_1 + j_2 + j_3 + j_4$, $\hat{\ell}_i = 2\ell_i + 1$, $\hat{j}_i = 2j_i + 1$, and $\mathcal{R}^L_{ij,Q} = \langle i|r^L|j\rangle_Q$ is the radial matrix element of atom Q. The $(\cdot)$ expressions represent Wigner-3j symbols, and the $\{\cdot\}$ expressions represent Wigner-6j symbols.

The diagonal elements, i.e., $|1A,2B\rangle = |3A,4B\rangle$, are given by

$$\begin{aligned}
\langle 1A,2B;\Omega|\hat{H}|1A,2B;\Omega\rangle &= \langle 1A,2B;\Omega|V_L(R)|1A,2B;\Omega\rangle \\
&+ E_{1A} + E_{2B}\,, \qquad (11)
\end{aligned}$$

where $\langle 1A,2B;\Omega|V_L(R)|1A,2B;\Omega\rangle$ follows (9) and (10), and each E_{iQ} is the asymptotic energy of the atomic Rydberg state $|n_i,\ell_i,j_i,m_{j_i}\rangle_Q$:

$$E_{iQ} = -\frac{1}{2(n_{iQ} - \delta_{\ell_i Q})}\,. \qquad (12)$$

In this expression, n_{iQ} is the principal quantum number of atom Q and $\delta_{\ell_i Q}$ is the quantum defect for atom Q (values given in [1], [39], and [40]).

III. INTERACTION CURVES

After investigating all possible Ω symmetries for the $70s + 70s$ and $70p + 70p$ excitations of rubidium and potassium, we found that in both cases the $\Omega = 0^+$ and the $\Omega = 0^-$ symmetries resulted in potential wells capable of supporting bound states. In Fig. 2, we plot the interaction energies for these four cases against the Bohr radius (a_0) and highlight the resulting potential wells in red; we also label the wells' corresponding asymptotic energy levels.

For all four of these wells, we explored scaling relations, composition, and stability. We provide a visual example in Fig. 3(a), where the potential well corresponding to the $\Omega = 0^+$ symmetry for both atoms excited to the $70s$ state is isolated. This well is ~600 MHz deep and supports ~630 bound vibrational states. In Table IV, we list the first few bound-state vibrational energies (as measured from the bottom of the well) for all four wells, as well as the classical turning points, indicating the large size of these dimer states. Given that the equilibrium separation R_e for all four wells is between 41 000a_0 and 46 000a_0 (~2.25 μm), these bound states are very extended, consistent with the *macrodimer* classification.

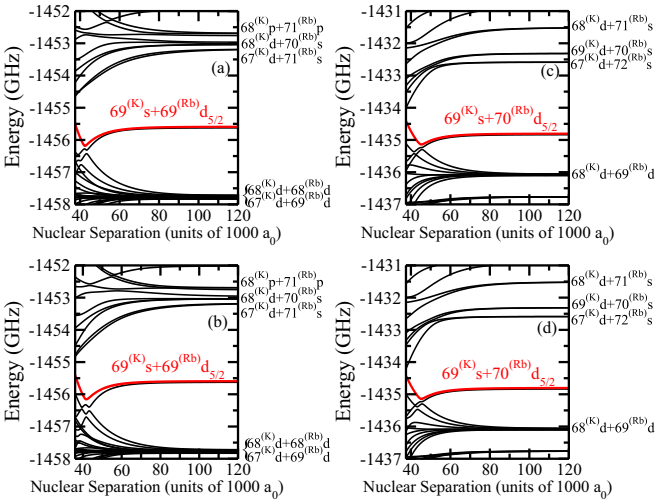

FIG. 2. Long-range potential energy curves corresponding to the interactions between one rubidium atom and one potassium atom excited to the same state. (a) Curves correspond to the $\Omega = 0^+$ symmetry with both atoms excited to the $70s$ state, (b) curves correspond to the $\Omega = 0^-$ symmetry with both atoms excited to the $70s$ state, (c) curves correspond to the $\Omega = 0^+$ symmetry with both atoms excited to the $70p$ state, and (d) curves correspond to the $\Omega = 0^-$ symmetry with both atoms excited to the $70p$ state. We highlight the potential energy wells in red and label their respective asymptotic states.

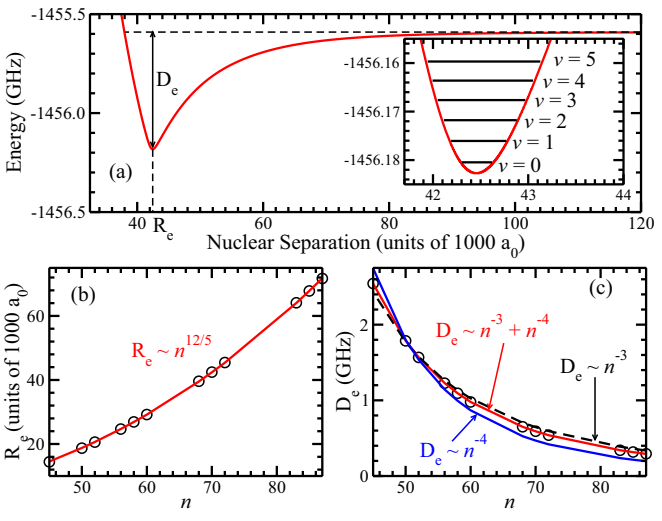

FIG. 3. (a) Long-range potential energy curves corresponding to the $\Omega = 0^+$ symmetry interactions of one potassium Rydberg atom and one rubidium Rydberg atom; both atoms have been excited to the $70s$ state. We note the existence of an ~600-MHz-deep well associated with the $69^{(\rm K)}s + 69^{(\rm Rb)}d_{5/2}$ asymptotic level, capable of supporting many bound states. We explicitly label the equilibrium separation R_e and the dissociation energy D_e. Inset: Zoom-in on the deepest part of the well, showing the first few bound vibrational levels; corresponding energies and classical turning points are listed in Table IV. (b) Scaling relations for the equilibrium separation R_e vs the principal quantum number n: $R_e \sim n^{12/5}$. (c) Scaling relations for the dissociation energy D_e vs the principal quantum number n. Three results (see text) are shown: $D_e \sim n^{-4}$ (blue line) gives a poor agreement, $D_e \sim n^{-3}$ (dashed black line) gives a good agreement, and $D_e \sim n^{-3} + n^{-4}$ (red line) gives the best agreement.

TABLE III. n-scaling relations for the equilibrium separation R_e and the dissociation energy D_e for the four potential wells discussed in this work (see Fig. 2). Both results are consistent with previous work regarding homonuclear macrodimers (see text).

Threshold energy (well)	Symmetry	R_e scaling	D_e scaling
$69^{(K)}s + 69^{(Rb)}d_{5/2}$	$\Omega = 0^+$	$n^{2.4}$ ($n^{12/5}$)	$n^{-3} + n^{-4}$
$69^{(K)}s + 69^{(Rb)}d_{5/2}$	$\Omega = 0^-$	$n^{2.4}$ ($n^{12/5}$)	$n^{-3} + n^{-4}$
$69^{(K)}s + 70^{(Rb)}d_{5/2}$	$\Omega = 0^+$	$n^{2.3}$	$n^{-3} + n^{-4}$
$69^{(K)}s + 70^{(Rb)}d_{5/2}$	$\Omega = 0^-$	$n^{2.3}$	$n^{-3} + n^{-4}$

The inset in Fig. 3(a) shows that the deepest part of the wells can be well modeled as a harmonic potential; the first few bound levels for each well are consistently spaced (see Table IV). The bound energies and corresponding wave functions were calculated using the mapped Fourier grid method [41] for each potential well individually.

A. Scaling relations

The dissociation energy D_e and the equilibrium separation R_e for the potential wells were calculated for various values of the principal quantum number n. In Figs. 3(b) and 3(c), we show the results for the $\Omega = 0^+$ symmetry with both atoms excited to the $70s$ state. In Fig. 3(b), we see that the equilibrium separation scales as $n^{12/5}$, and in Fig. 3(c), we present different "best-fit" curves corresponding to different values of n scaling for the dissociation energy. For pure dipole-dipole coupling, one would expect the dissociation energy to scale as the energy difference between energy levels (n^{-3} for Rydberg atoms [1]). We see that this result gives a pretty good agreement, but the results suggest that D_e actually scales as $\sim n^{-4} + n^{-3}$. Although it gives a poor agreement, we also include the curve of n^{-4} for completeness. In Table III, we list the scaling results for all four of the potential wells identified in Fig. 2. We note that the scaling results obtained here for R_e and D_e are consistent with the results for homonuclear macrodimers, presented in [10]. A thorough derivation for these scaling relations was also performed in that work; we do not republish it here.

B. Well composition and stability

Due to the electronic ℓ mixing, each potential energy curve $U_\lambda(R)$ is described by an electronic wave function $|\chi_\lambda(R)\rangle$, which itself is a superposition of the asymptotic molecular wave functions (4):

$$|\chi_\lambda(R)\rangle = \sum_j c_j^{(\lambda)}(R)|j\rangle \ . \tag{13}$$

The exact amount of mixing varies with R and is completely described by the $c_j^{(\lambda)}(R)$ coefficients: the eigenvectors after diagonalization. The $|j\rangle$ are the corresponding symmetrized basis states $|1A,2B;\Omega\rangle$ defined earlier, (4). As an example of the R dependence of the mixing, in Fig. 4(b) we illustrate the composition of the potential well highlighted in Figs. 3(a) and 4(a). This potential curve corresponds to the $69^{(K)}s + 69^{(Rb)}d_{5/2}$ asymptote.

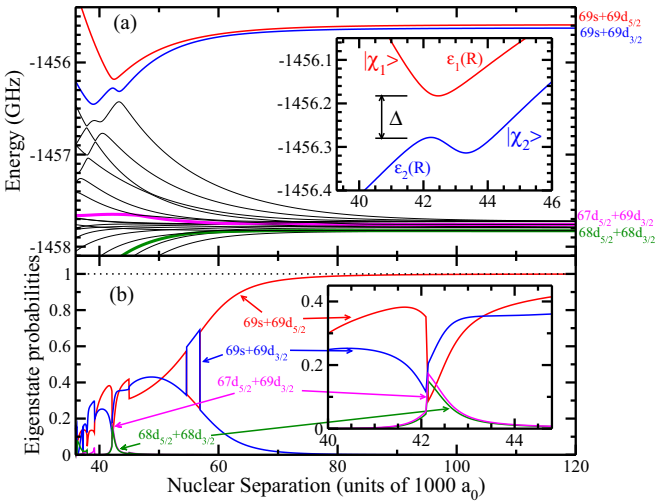

FIG. 4. (a) $\Omega = 0^+$ potential energy curves describing the interactions between one potassium Rydberg atom and one rubidium Rydberg atom: both atoms have been excited to the $70s$ state. We highlight curves corresponding to the electronic states that contribute the most to the formation of the well (see text). Inset: Zoom-in on the region near the avoided crossing, indicating the relevant features of the Landau-Zener treatment: Δ is the energy gap between the adiabatic energies ϵ_1 and ϵ_2 at closest approach; these adiabatic energies correspond to the two adiabatic states $|\chi_1\rangle$ and $|\chi_2\rangle$ at the avoided crossing. (b) Probabilities $|c_j(R)|^2$ of the electronic basis states $|j\rangle$ most responsible for the formation of the well (see text). After $\sim$60 000a_0, the ℓ mixing is negligible: the probability coefficient corresponding to $69^{(K)}s + ^{(Rb)}\ 70d_{5/2}$ approaches 1 (see dashed line) and all other probability coefficients decay to 0. Inset: Zoom-in on the region near the avoided crossing. All panels use the same labeling and/or color scheme.

As would be expected, this well is mainly composed of the $69^{(K)}s + 69^{(Rb)}d_{5/2}$ state. However, in the region of the actual well, we also see significant contributions from the $69^{(K)}s + 69^{(Rb)}d_{3/2}$ directly below the well and even from some deeper $nd + n'd$ states. In Fig. 4(a), we highlight and label the four states most relevant to ℓ mixing; the corresponding probabilities $|c_j(R)|^2$ of these states are plotted against R in Fig. 4(b) to explicitly describe the R dependence. We note that the effects from ℓ mixing cease when the nuclear separation is about 60 000a_0. This is obvious because the probability coefficient of the $69^{(K)}s + 69^{(Rb)}d_{5/2}$ state approaches 1, while all other coefficients approach 0. Also of note is the switch in probabilities of the $69^{(K)}s + 69^{(Rb)}d_{5/2}$ and $69^{(K)}s + 69^{(Rb)}d_{3/2}$ states between $\sim$55 000a_0 and $\sim$57 000a_0. Although perhaps not visually obvious in Fig. 4(a), these two curves do appear to experience an avoided crossing in this general vicinity: one can observe a slight deviation in the line shapes of these two curves as they meet. Such a crossing would be consistent with the behavior of the probabilities.

For potential energy wells formed via some avoided crossing between curves, predissociation of bound energy levels can be a concern. In general, avoided crossings can lead to predissociation if the (meta-)stable state has strong coupling to the unstable state below it. From the eigenvector plot in Fig. 4(b), we see that there is significant coupling between the

TABLE IV. Energies of the deepest bound levels (measured from the bottom of the well), classical turning points (R_1, R_2), and dimer lifetimes τ (see text) for the four potential wells identified in Fig. 2.

Excited Rydberg pair	Threshold energy (well)	Symmetry	v	Energy (MHz)	R_1 (a.u.)	R_2 (a.u.)	τ (s)
$70^{(K)}s + 70^{(Rb)}s$	$69^{(K)}s + 69^{(Rb)}d_{5/2}$	$\Omega = 0^+$	0	2.2240	42 175	42 783	∞
			1	6.6490	42 175	42 784	∞
			2	10.9194	42 095	42 891	∞
			3	15.0636	42 031	42 985	∞
			4	19.0879	41 976	43 070	∞
			5	23.0177	41 926	43 149	∞
			⋮	⋮	⋮	⋮	⋮
			627	591.9279	37 967	226 597	∞
$70^{(K)}s + 70^{(Rb)}s$	$69^{(K)}s + 69^{(Rb)}d_{5/2}$	$\Omega = 0^-$	0	1.7120	41 591	41 983	∞
			1	5.1375	41 456	42 145	∞
			2	8.5053	41 366	42 260	∞
			3	11.8269	41 292	42 360	∞
			4	15.0967	41 232	42 447	∞
			5	18.3146	41 177	42 527	∞
			⋮	⋮	⋮	⋮	⋮
			608	564.7000	37 067	157 474	∞
$70^{(K)}p + 70^{(Rb)}p$	$69^{(K)}s + 70^{(Rb)}d_{5/2}$	$\Omega = 0^+$	0	1.3422	45 088	45 535	∞
			1	3.9897	44 937	45 718	∞
			2	6.5859	44 834	45 854	∞
			3	9.1309	44 750	45 970	∞
			4	11.6247	44 681	46 073	∞
			5	14.0752	44 620	46 169	∞
			⋮	⋮	⋮	⋮	⋮
			470	335.6738	40 716	181 441	∞
$70^{(K)}p + 70^{(Rb)}p$	$69^{(K)}s + 70^{(Rb)}d_{5/2}$	$\Omega = 0^-$	0	1.3682	45 072	45 512	∞
			1	4.0782	44 921	45 696	∞
			2	6.7330	44 821	45 832	∞
			3	9.3245	44 739	45 947	∞
			4	11.8687	44 670	46 050	∞
			5	14.3575	44 608	46 147	∞
			⋮	⋮	⋮	⋮	⋮
			473	337.7708	40 746	158 929	∞

potential well and the curves that lie below it. Therefore, the long-term stability of these wells could be compromised.

For curves that are less intricate, a simple Landau-Zener (LZ) [42,43] treatment would be desirable. However, such an approach depends on detailed knowledge of the *diabatic* crossing behavior, including which diabatic states actually correspond to the crossing potential energy curves; for the complicated curve mixings that we demonstrate, defining these diabatic states becomes difficult. Instead, we adopt the approach taken by Clark [44], in which the parameters defining the Landau-Zener probability are obtained from the adiabatic P-matrix coupling. Specifically, the P matrix is defined through the off-diagonal derivative of the interaction potential between the crossing states:

$$P_{12}(R) = \frac{\langle \chi_1 | (\partial/\partial R) V(R) | \chi_2 \rangle}{(\varepsilon_1(R) - \varepsilon_2(R))} . \tag{14}$$

Here, $\varepsilon_i(R)$ is the energy value of the adiabatic potential curve described by state $|\chi_i\rangle$, and $V(R)$ is defined by Eq. (8). As the nuclear separation is varied, the value of the P matrix peaks when the adiabatic curves are at their closest approach [corresponding to $\varepsilon_1(R) - \varepsilon_2(R)$ being a minimum]. Clark showed that by fitting the P matrix to a Lorentzian function, the probability that $P_{\rm LZ}$ will make a nonadiabatic transition from the electronic state $|\chi_1\rangle$ to the electronic state $|\chi_2\rangle$ is given by

$$P_{\rm LZ} = \exp\left(-\frac{2\pi}{v} \frac{\Delta}{8\, P_{\rm max}} \right) , \tag{15}$$

where v is the relative velocity of the two nuclei determined from the bound levels of the molecule, Δ is the energy gap between the two adiabatic curves at closest approach, and $P_{\rm max}$ is the peak value of the P matrix. The inset in Fig. 4(a) shows a closeup of the avoided crossing between the $|\chi_1\rangle \equiv 69^{(K)}s + 69^{(Rb)}d_{5/2}$ and the $|\chi_2\rangle \equiv 69^{(K)}s + 69^{(Rb)}d_{3/2}$ electronic states; the energy gap Δ is also indicated.

Since $P_{\rm LZ}$ represents the likelihood of transitioning from $|\chi_1\rangle$ to $|\chi_2\rangle$ (and thus predissociating into two free atoms), $1 - P_{\rm LZ}$ is the probability that the macrodimer will remain in $|\chi_1\rangle$ and *not* predissociate. We match this probability to an

exponential decay over the time t for a full oscillation inside the well, $1 - P_{LZ} = e^{-t/\tau}$, and find τ, the "lifetime" of the dimer; the results are summarized in Table IV.

Our calculations show that all of the bound states have near-zero P_{LZ} values and thus near-infinite lifetimes. Although there is strong coupling between the well and the states below it, the energy gap between the well and the lower curves is too large for dissociation to occur. In addition, the oscillation speeds of the dimers are too slow for diabatic transitions. We therefore conclude that these dimers are stable with respect to predissociation and so their lifetime is limited only by the Ryberg atoms themselves ($t_{Ryd} \sim 700\ \mu$s for $n = 70$) [45].

IV. CONCLUSIONS

In this paper, we investigated the long-range interactions between rubidium and potassium, where both atoms are excited to high-n Rydberg states. We explored all possible Ω symmetries for both atoms being excited to the $70s$ state and the $70p$ state. Our calculations showed that due to the effects of electronic ℓ mixing, the potential energy curves describing these interactions are intricate and complicated, particularly when the nuclear separations are in the $40\ 000a_0$–$60\ 000a_0$ range. In addition, when both atoms are excited to either the $70s$ state or the $70p$ state, both the $\Omega = 0^+$ symmetry interactions and the $\Omega = 0^-$ symmetry interactions result in potential wells capable of supporting many bound states. We analyzed these wells in detail, calculating the bound vibrational levels, the stability of these levels, and various n-scaling relations.

Given the interest in photoassociation experiments between different alkali species, these results could be useful for further ultracold experiments, quantum chemistry calculations, and/or quantum information research. Furthermore, it might be possible to exploit the ℓ mixing for application to "dressed" Rydberg states [46,47].

[1] T. Gallagher, *Rydberg Atoms* (Cambridge University Press, Cambridge, UK, 1994).
[2] W. R. Anderson, J. R. Veale, and T. F. Gallagher, Phys. Rev. Lett. **80**, 249 (1998).
[3] I. Mourachko, D. Comparat, F. de Tomasi, A. Fioretti, P. Nosbaum, V. M. Akulin, and P. Pillet, Phys. Rev. Lett. **80**, 253 (1998).
[4] S. M. Farooqi, D. Tong, S. Krishnan, J. Stanojevic, Y. P. Zhang, J. R. Ensher, A. S. Estrin, C. Boisseau, R. Côté, E. E. Eyler, and P. L. Gould, Phys. Rev. Lett. **91**, 183002 (2003).
[5] K. R. Overstreet, A. Schwettmann, J. Tallant, and J. P. Shaffer, Phys. Rev. A **76**, 011403 (2007).
[6] C. H. Greene, A. S. Dickinson, and H. R. Sadeghpour, Phys. Rev. Lett. **85**, 2458 (2000).
[7] V. Bendowsky, B. Butscher, J. Nipper, J. P. Shaffer, R. Löw, and T. Pfau, Nature **458**, 1005 (2009).
[8] C. Boisseau, I. Simbotin, and R. Côté, Phys. Rev. Lett. **88**, 133004 (2002).
[9] N. Samboy, J. Stanojevic, and R. Côté, Phys. Rev. A **83**, 050501 (2011).
[10] N. Samboy and R. Côté, J. Phys. B **44**, 184006 (2011).
[11] K. R. Overstreet, A. Schwettmann, J. Tallant, D. Booth, and J. P. Shaffer, Nature Phys. **5**, 581 (2009).
[12] M. D. Lukin, M. Fleischhauer, R. Cote, L. M. Duan, D. Jaksch, J. I. Cirac, and P. Zoller, Phys. Rev. Lett. **87**, 037901 (2001).
[13] M. Saffman, T. G. Walker, and K. Mølmer, Rev. Mod. Phys. **82**, 2313 (2010).
[14] L. G. Marcassa and J. P. Shaffer, in *Advances in Atomic and Molecular Physics* (Academic Press, San Diego, CA, 2014), pp. 47–133.
[15] S. T. Rittenhouse, M. Mayle, P. Schmelcher, and H. R. Sadeghpour, J. Phys. B **44**, 184005 (2011).
[16] S. T. Rittenhouse and H. R. Sadeghpour, Phys. Rev. Lett. **104**, 243002 (2010).
[17] I. C. H. Liu and J. M. Rost, Eur. Phys. J. D **40**, 65 (2006).
[18] I. C. H. Liu, J. Stanojevic, and J. M. Rost, Phys. Rev. Lett. **102**, 173001 (2009).
[19] N. Samboy and R. Côté, Phys. Rev. A **87**, 032512 (2013).
[20] M. Kiffner, W. Li, and D. Jaksch, Phys. Rev. Lett. **111**, 233003 (2013).
[21] M. Kiffner, M. Huo, W. Li, and D. Jaksch, Phys. Rev. A **89**, 052717 (2014).
[22] C. L. Vaillant, M. P. A. Jones, and R. M. Potvliege, J. Phys. B **45**, 135004 (2012).
[23] S. Ye, X. Zhang, T. C. Killian, F. B. Dunning, M. Hiller, S. Yoshida, S. Nagele, and J. Burgdörfer, Phys. Rev. A **88**, 043430 (2013).
[24] F. Camargo, J. D. Whalen, R. Ding, H. R. Sadeghpour, S. Yoshida, J. Burgdörfer, F. B. Dunning, and T. C. Killian, Phys. Rev. A **93**, 022702 (2016).
[25] J. Banerjee, D. Rahmlow, R. Carollo, M. Bellos, E. E. Eyler, P. L. Gould, and W. C. Stwalley, J. Chem. Phys. **139**, 174316 (2013).
[26] J. Banerjee, D. Rahmlow, R. Carollo, M. Bellos, E. E. Eyler, P. L. Gould, and W. C. Stwalley, J. Chem. Phys. **138**, 164302 (2013).
[27] T. Calarco, H. Briegel, D. Jaksch, J. Cirac, and P. Zoller, J. Mod. Opt. **47**, 2137 (2000).
[28] K. G. H. Vollbrecht, E. Solano, and J. I. Cirac, Phys. Rev. Lett. **93**, 220502 (2004).
[29] R. J. LeRoy, Can. J. Phys. **52**, 246 (1974).
[30] J. Stanojevic, R. Côté, D. Tong, S. Farooqi, E. Eyler, and P. Gould, Eur. Phys. J. D **40**, 3 (2006).
[31] J. Stanojevic, R. Côté, D. Tong, E. E. Eyler, and P. L. Gould, Phys. Rev. A **78**, 052709 (2008).
[32] P. Bernath, *Spectra of Atoms and Molecules* (Oxford University Press, New York, 2005).
[33] J. Brown and A. Carrington, *Rotational Spectroscopy of Diatomic Molecules* (Cambridge University Press, Cambridge, UK, 2003).
[34] M. E. Rose, J. Phys. Math. **37**, 215 (1958).
[35] R. J. Buehler and J. O. Hirschfelder, Phys. Rev. **83**, 628 (1951).
[36] B. C. Carlson and G. S. Rushbrooke, Math. Proc. Cambr. Philos. Soc. **46**, 626 (1950).

[37] P. R. Fontana, Phys. Rev. **123**, 1865 (1961).
[38] A. Schwettmann, J. Crawford, K. R. Overstreet, and J. P. Shaffer, Phys. Rev. A **74**, 020701 (2006).
[39] W. Li, I. Mourachko, M. W. Noel, and T. F. Gallagher, Phys. Rev. A **67**, 052502 (2003).
[40] J. Han, Y. Jamil, D. V. L. Norum, P. J. Tanner, and T. F. Gallagher, Phys. Rev. A **74**, 054502 (2006).
[41] V. Kokoouline, O. Dulieu, R. Kosloff, and F. Masnou-Seeuws, J. Chem. Phys. **110**, 9865 (1999).
[42] L. Landau and E. Lifshitz, *Quantum Mechanics (Non-relativistic Theory)*, 3rd ed. (Pergamon Press, Oxford, UK, 1997).
[43] C. Zener, Proc. R. Soc. London A **137**, 696 (1932).
[44] C. W. Clark, Phys. Lett. A **70**, 295 (1979).
[45] I. I. Beterov, I. I. Ryabtsev, D. B. Tretyakov, and V. M. Entin, Phys. Rev. A **79**, 052504 (2009).
[46] J. E. Johnson and S. L. Rolston, Phys. Rev. A **82**, 033412 (2010).
[47] S. Helmrich, A. Arias, N. Pehoviak, and S. Whitlock, J. Phys. B **49**, 03LT02 (2016).